Elucidating Multiple Negative Differential Resistance and Rectification Ratio Through L-Aspartic Acid at Nanometre Scale Using Symmetrical Metal Electrodes

Gaurav Sikri (er.gaurav19@gmail.com)
Guru Nanak Dev University Amritsar Punjab India https://orcid.org/0000-0002-7151-4557
Ravinder Singh Sawhney
Guru Nanak Dev University

Research Article

Keywords: L-Aspartic acid, Amino acid, work function, tunnelling barrier, Molecular rectifier, Negative differential resistance

Posted Date: June 7th, 2021

DOI: https://doi.org/10.21203/rs.3.rs-548169/v1

Abstract

Protein-based electronics is one of the growing areas of bio-nanoelectronics, where novel electronic devices possessing distinctive properties, are being fabricated using specific proteins. Furthermore, if the bio-molecule is analysed amidst different electrodes, intriguing properties are elucidated. This research article investigates the electron transport properties of L-aspartic acid (i.e., L-amino acid) bound to symmetrical electrodes of gold, silver, copper, platinum and palladium employing NEGF-DFT approach using self-consistent function. The theoretical work function of different electrodes is calculated using local density approximation and generalized gradient approximation approach. The calculated work function correlates well with the hole tunnelling barrier and conductance of the molecular device, which further authenticate the coupling strength between molecule and electrode. Molecule under consideration also exhibits the multiple negative differential resistance and rectification ratio with all the different electrodes, due to its asymmetrical structure. The molecular device using platinum electrodes exhibits the highest peak to valley ratio of 1.38 and rectification ratio of 3.20, at finite bias. The switching characteristics of different molecular device are justified with detailed transmission spectra and MPSH. These results indicate that L-aspartic acid and similar biomolecule can be vital to the growth of Proteotronics.

1. Introduction

Biomolecules have evoked substantial attention among researchers due to their immense applications in nanoelectronic devices [1–10]. Such biomolecules exhibit the redox process and optical functionality in biological environment. Electrical charge in such biomolecules is generally transported by ions. The research is inclined towards the biomolecules acting as bridge between donor and acceptor moieties to form bio-nanoelectronic devices[11]. Proteins (from the Greek word Protos, i.e. of primary importance) are the bio-molecules that offer the distinctive optical and electronic properties. Due to biological existence, intense research has been focussed on charge transfer in proteins. In order to design practical bio-nanoelectronic devices, investigation of their electron transport properties is highly imperative. Electronic rectification in protein-based devices has evolved into a challenge for the researchers working in the field of bio-nanoelectronic[12]. Proteotronics has emerged as an essential branch to study the electron transport properties of proteins for new bio-nanoelectronic devices[13]. Although, there is significant connection between electron transfer (ET) and electron transport (ETp) properties[14, 15], yet there is a sense of ambiguity to predict the exact mechanism of electron transport through proteins [16, 17]. The emphatic potency of proteins can be predicted, if the building blocks of proteins (i.e., amino acids) are intrigued individually.

Among 20 amino acids, only two (i.e., L-glutamic acid and L-aspartic acid) are negatively charged. Different L-amino acids are distinguished by their distinct side chain structures[18]. Charged amino acids are the major determinants of the rectification of gap junctional channel [19] and short-range ET and ETp [20]. Current rectification is observed in asymmetric molecule structures [21–24] and due to the molecule-electrode coupling [25].

In our previous work, we examined the transport properties of L-glutamic acid (i.e. $C_5H_9NO_4$) [26]. In this research work, L-aspartic acid (i.e., L-amino acid) $C_4H_7NO_4$, is molecule of choice due to the presence of asymmetrical alkane carbon chain[27, 28]. L-amino acid acts as a transmitter for central nervous system of mammals and is being exceedingly used in biosynthesis of proteins [29]. Asymmetric structure of the L-aspartic acid crystal has been observed using atomic force microscopy [30]. Carboxylic acid side-chain has an important role to play in the conductivity of the amino acids [20]. This side chain can also influence the long-distance electron transfer in peptides [31].

Certain amino acids have attained special attention due to their unique transport properties [32–36]. These molecules are rigidly attached to atomic scale electrodes to form molecular junctions[37]. Furthermore, finite bias is applied across electrodes to investigate electronic transport behaviour of such molecules. The distinctive electronic behaviour confirms the candidature of such molecules for future electronic devices [24].

Besides proteins, extensive research has been carried out about bio-nanoelectronic devices consisting of building blocks (i.e. L-amino acids) in peptides [38], homopeptides [39], polypeptides [40, 41]. Moreover, peptides can be engineered to create modified protein structures [42].

Biomolecules show different current-voltage (I-V) characteristics with different electrodes [43–45]. In our previous work, we elucidated electronic transport properties of L-glutamic acid stringed to gold, silver and copper electrodes [26]. We move a step forward towards investigating negatively charged L-amino acid (i.e. L-aspartic acid) with two additional metallic electrodes of platinum and palladium. We also focus on the correlation of metal work function and molecule-electrode coupling in this research work.

2. Theory And Simulations

Presently, lot of focus is on developing molecular devices particularly containing bio-molecule. Specifically, amino acids are getting utmost attention among researchers to develop distinct bio-nanoelectronic devices [24]. We have assembled five different device configurations with central scattering region comprising of L-aspartic molecule attached to semi-infinite metallic electrodes. The metallic electrodes are assumed to be ballistic conductors having unity probability of transmission. These electrodes accept all the carrier flow from the channel and avoid backscattering into the channel [46].

In order to achieve non-equilibrium, a finite bias is applied across the junctions using Landauer's approach [47]. The metallic electrodes for this research work are prepared using (1, 1, 1) miller indices. We observe that copper, platinum and palladium electrodes exhibit 6 layers in comparison to 3 layers in gold and silver electrodes. Such increase in layers is due to smaller inter-atomic distance of the respective electrodes. For the sake of comparing some significant parameters, we have used the fixed size simulation box of such electrodes and considered only 3 layers for all the electrodes as shown in Fig.1 (a-e).

Though numerous fabrication techniques have been listed in literature for fabricating molecular junctions, but we have theoretically employed mechanically control break junction (MCBJ) approach for its simplicity and effective results [48]. This technique is based on the stretching the wire, until the junction breaks and gives two separate electrodes. Relaxing the force on the elastic substrate by back-bending allows the junction to be closed again [49]. This technique also offers the possibility to vary the contact geometry and contact resistance between molecule and electrodes [50].

The transport properties of proposed molecular devices are investigated employing a combination of DFT and non-equilibrium Green's function (DFT-NEGF), which has emerged as workhorse for many mathematical modelling calculations in last two decades [51, 52]. This study has been carried out using Atomistic Tool Kit-Virtual Nano Lab (ATK-VNL) software [53] which is based on Gaussian basis set and TranSiesta-C.

The electron exchange correlation has been described employing the Perdew–Burke–Ernzerhof (PBE) [54] version of the generalized gradient approximation (GGA) that foremost fulfils the several mathematical requirements of DFT [55]. PBE suggests good trade-off between computational efforts and precision in amino acids and oligopeptides [56]. A combination of Double-Zeta Plus polarization (DZP) basis set and PBE-GGA has been excessively studied for environmental stability [57] and bio-sensing [58] of amino acids. However, we have employed Double-Zeta Double Polarized basis sets for the purpose of extending wave functions [59]. The atomic calculations are performed using norm-conserving Troullier–Martins pseudo-potentials [60]. The Monkhorst–Pack k-point sampling of 1x1x100 points along with mesh cutoff energy of 75 Hartree is employed for our mathematical calculations.

3. Results And Discussions

Firstly, we focus on the theoretical work function of the different metal electrodes. Theoretical prediction of work function offers a convenient and complementary tool to cumbersome experiment. Nevertheless, these predictions are not perfect due to approximations that are meant to make theory tractable [61]. Work function is the minimum energy required to remove an electron from the Fermi level to a state where it is at rest, without interacting with the solid. It is the type of binding energy which is equal to energy difference between the vacuum level and the Fermi level. Chemically, it is defined as the difference between ionization potential and HOMO energy [62]. We initiated our research with local density approximation (LDA) and GGA for predicting work functions of the different electrodes using 9x9x1 k-point sampling given in Table 1. Experimental as well as theoretical values of work function reported by other researchers are also given in Table 1. Both LDA and GGA are found to yield excellent agreement of work function with other experimental and theoretical values with lesser error estimates[63–78].

If we scrutinize the electrodes on the basis of work function, we found that Au(111) and Pt(111) offers the maximum and Cu(111) offers the minimum work function in both LDA and GGA. We extend our further research using GGA as it gives balanced descriptions of structures and energies with overall improvement over LDA [67, 74].

Next, we focus on the energy offset between dominant molecular orbital and Fermi energy (E_f), which is used to predict the tunnelling barrier. In our theoretical modelling of Aspartic acid with different electrodes, the Highest Occupied Molecular Orbital (HOMO) lies closer to Fermi energy, providing the Hole tunnelling barrier. The Hole tunnelling barrier (HTB) can be given as where is the HOMO energy level of the molecular device. The HTB of l-Aspartic acid within different electrodes is given in fig 1(f).

Table 1 Work functions (eV) of different metallic electrodes

Metal	Others Experimental Work Function	Others Theoretical Work Function		Our Theoretical Work Function	
		LDA	GGA	LDA	GGA
Au(111)	5.26[75], 5.33±0.06 [63], 5.3 to 5.6[76]	5.49[65], 5.63[77]	5.12[65], 5.15 [78]	5.28	4.99
Ag(111)	4.56[75], 4.53±0.07 [63], 4.74[64], 4.75±0.01[68]	4.84[69], 4.97[65]	4.49[65]	4.78	4.22
Cu(111)	4.94[75], 4.9±0.02 [63], 4.94[70]	5.20[65]	4.88[65]	4.31	4.11
Pt(111)	5.82[75], 5.91±0.08 [63], 6.08±0.15[71]	6.08[65], 6.06[72]	5.72[65], 5.69[78]	5.21	5.08
Pd(111)	5.55[75], 5.67±0.12 [63], 5.44±0.03[73]	5.66[65], 5.64[72]	5.32[65], 5.25[78]	4.75	4.15

There is significant correlation between work function and tunnelling barrier of the molecular junctions. The Electrodes with higher work function result in lower tunnelling barriers [79]. This is clearly acceptable in our case as Pt (111) and Au (111) offers the maximum work function and Au-Aspartic-Au and Pt-Aspartic-Pt offers the minimum HTB. The lower tunnelling barrier of molecular device offers the stronger coupling between molecule and the electrode [80].

Next, we measure the conductance across the proposed molecular devices, which is expressed as , where is the significant quantum conductance unit and is the transmission coefficient of the channel. The value of i.e., , where is the elementary charge and is the Planck constant [81]. We notice that the conductance dip is visible in Ag-Aspartic-Ag and Cu-Aspartic-Cu devices as shown in Fig. 1(h) and (i). This is due to weak coupling of molecule to the specific electrode [82].

The conductance remains quantized within the finite bias range of -0.2 to +0.2V, -0.6 to +0.4V and -0.6 to +0.6V in case of Au-Aspartic-Au, Ag-Aspartic-Ag and Cu-Aspartic-Cu devices, shown in Fig.1(g, h and i) respectively. This quantized conductance implies insensitivity of the respective devices at specific bias range [83, 84]. Further, this insensitivity can lead to almost I-V characteristics of such devices within the same bias region.

The highest conductance peak appears at +0.2 V in case of Pt-Aspartic-Pt device. The molecule exhibits the least conductance with Cu-Aspartic-Cu device within the finite bias range of -2 to +2V. In case of Pd-

Aspartic-Pd device, the conductance shows fluctuations of varying magnitude. The zero bias conductance of the proposed molecular devices follow the order as Pt-Aspartic-Pt (0.1184 G0) > Pd-Aspartic-Pd (0.0751 G0) > Au-Aspartic-Au (0.0650 G0) > Ag-Aspartic-Ag (0.0114 G0) >Cu-Aspartic-Cu (0.0034 G0). Different amino acids including l-aspartic acid, offers very less conductance even in experimental MCBJ techniques [32].

The coupling strength and the HTB between the electrodes and the molecule significantly influence the conductance of the molecular junction [85]. The zero bias conductance of different molecular devices correlates well with the work function of the metal electrodes based on GGA. The zero bias conductance is maximum in Pt-Aspartic-Pt and minimum in Cu-Aspartic-Cu.

Next, we observe the I-V characteristics and calculate the rectification ratios (RR) of all the proposed molecular devices in finite bias range of -2 to +2V. The current is approximately equal to integration of transmission coefficient within the bias window ranging from to , where is the magnitude of the bias voltage. The three- dimensional transmission spectra of the proposed molecular devices within the bias range of −2 to +2V is shown in the Fig.1 (l-p). The dotted black lines indicate the bias window. The molecule exhibits finite negative differential resistance (NDR) and RR with all the five electrodes.

In case of Au-Aspartic-Au device, the current changes almost linearly in the bias range of -0.8 to +0.8V as depicted in Fig. 2 (a). Three different NDR regions are observed in the different bias ranges. We noticed peak to valley ratio, ηg1= 1.33 with peak voltage (Vp) of 0.8V and valley voltage (Vv) of 1.2 V in case of Au-Aspartic-Au device. The other two NDR peaks observed in device using gold electrode as ηg2=1.21 (with Vp=1.8V, Vv=2.0V) and ηg3=1.27 (with Vp=-1.4V, Vv=-2.0V).

In case of Ag-Aspartic-Ag device, two instances of NDR are observed in only positive bias as ηs1=1.26 (with Vp=1.0V, Vv=1.4V) and ηs2=1.07(with Vp=1.6V, Vv=1.8V) shown in Fig. 2 (b). In case of Cu-Aspartic-Cu device, three different instances of NDR are observed as ηc1= 1.19 (with Vp=1.8 V, Vv=2V), ηc2= 1.03 (Vp=-1.2V, Vv=-1.4 V) and ηc3=1.18(Vp=-1.6 V, Vv=-1.8V) shown in Fig. 2 (c). In case of Pt-Aspartic-Pt device, five distinct NDR peaks are observed as ηpt1=1.14 (Vp=0.2 V, Vv=0.4V), ηpt2=1.38 (Vp=0.6 V, Vv=0.8 V), ηpt3=1.06 (Vp=1.0, Vv=1.2V), ηpt4=1.14 (Vp=1.8V, Vv=2.0V) and ηpt5=1.09 (Vp=-1.2V, Vv=-1.4V) as depicted in Fig. 2 (d). In case of Pd-Aspartic-Pd device, six distinct NDR peaks are observed as ηpd1= 1.05 (Vp=0.6V, Vv=0.8V), ηpd2=1.29 (Vp=1.2 V, Vv=1.4V), ηpd3=1.32 (Vp=1.6V, Vv=1.8V), ηpd4= 1.02 (Vp=-0.2V, Vv=-0.4V), ηpd5=1.01(Vp=-1.2V, Vv=-1.4V) and ηpd6=1.15(Vp=-1.6V, Vv=-2.0) as shown in Fig. 2 (e).

The flat conductance observed in both Ag-Aspartic-Ag device (i.e. from -0.6 to +0.4V) and Cu-Aspartic-Cu device (i.e. from -0.6 to +0.6V) (shown in Fig. 1 (h) and (i)) has insightful effect on their IV characteristics, (shown in Fig. 2 (b) and (c)) as the current does not show any significant rise within this specific bias range.

In case of Au-Aspartic-Au device, the molecule exhibits the highest rectification ratio of 1.89 at ±1.4 V as shown in inset of Fig 2 (a). As the bias voltage sweeps from 0.6 to 1.4 V, the rectification ratio increases

with increase in bias voltage and then decreases with increase in bias voltage from 1.4 to 1.8V. This is due to the shifting of transmission peaks within the bias window with respect to change in bias voltage as shown in Fig.1 (l).

The molecule exhibits the highest rectification ratio of 1.81 (at ±1.8 V), 1.31 (at ± 2V), 3.20 (at ±0.2 V) and 1.87 (at ±0.4 V) with silver, copper, platinum and palladium electrodes, respectively shown in inset of Fig. 2 (b), (c), (d), and (e).

The NDR and rectifying behaviour of the device can be pointed by transmission spectra, which is the most significant representation of quantum transport behaviour. The appearance of transmission peaks within the bias window (shown in Fig. 1(l-p)) can be attributed to the enhancement of current.

The I-V range for molecular devices at finite bias range of –2 to +2V, increases as the electrode work function increases. The Cu-Aspartic-Cu has minimum I-V range but Pt-Aspartic-Pt has maximum I-V range. Junctions with higher contact resistance have smaller coupling strength [86]. The higher the work function, the closer is the HOMO to the Fermi level, smaller is the offset between HOMO and Fermi energy (i.e. HTB) and the stronger is the molecule-electrode coupling [80].

We now focus on the cause of the highest NDR and RR of respective devices. In Fig. 2(f), (g), (i) and (j) the area under the curve decreases with increase in bias voltage, which causes the existence of NDR behaviour. In Fig. 2(h), the HOMO shifts away from the vicinity of Fermi level with increase in bias voltage from 1.8 to 2.0V. This shift causes the destruction of HOMO to split into HOMO and HOMO-1 resonances, which causes the NDR behaviour.

In case of Au-Aspartic-Au device, the area covered under HOMO and HOMO-1 resonant peaks at -1.4V is more as compared to +1.4V, reflecting the cause of rectification ratio as shown in Fig. 2 (k). In case of Ag-Aspartic-Ag device, though HOMO of +1.8V is near to the Fermi level, yet the combination of HOMO and HOMO-1 of -1.8V is more effective to show more current shown in Fig. 2 (l).

In case of Cu-Aspartic-Cu device, the closeness of HOMO near the Fermi level at -2.0V depicts more current than +2.0 V as shown in Fig.2 (m). The area covered under the bias voltage of +0.2V and +0.4V is higher than -0.2V and -0.4 V in Pt-Aspartic-Pt and Pd-Aspartic-Pd devices, respectively shown in Fig. 2 (n) and (o). This clearly explains the cause of rectification ratio.

In order to emphasize more on the cause of rectification ratio, we need to focus on the Molecular Projected Self-consistent Hamiltonian (MPSH) states of proposed molecular devices. In Table 2, the bias voltage of -1.4 V shows more delocalization at HOMO-1 as compared to +1.4 V in Au-Aspartic-Au device, justifying the rectification ratio.

Table 2 (Color online) MPSH states of Au-Aspartic-Au at ±1.4V, Ag-Aspartic-Ag at ±1.8V, Cu-Aspartic-Cu at ±2 V, Pt-Aspartic-Pt at ±0.2 V, and Pd-Aspartic-Pd at ±0.4V.

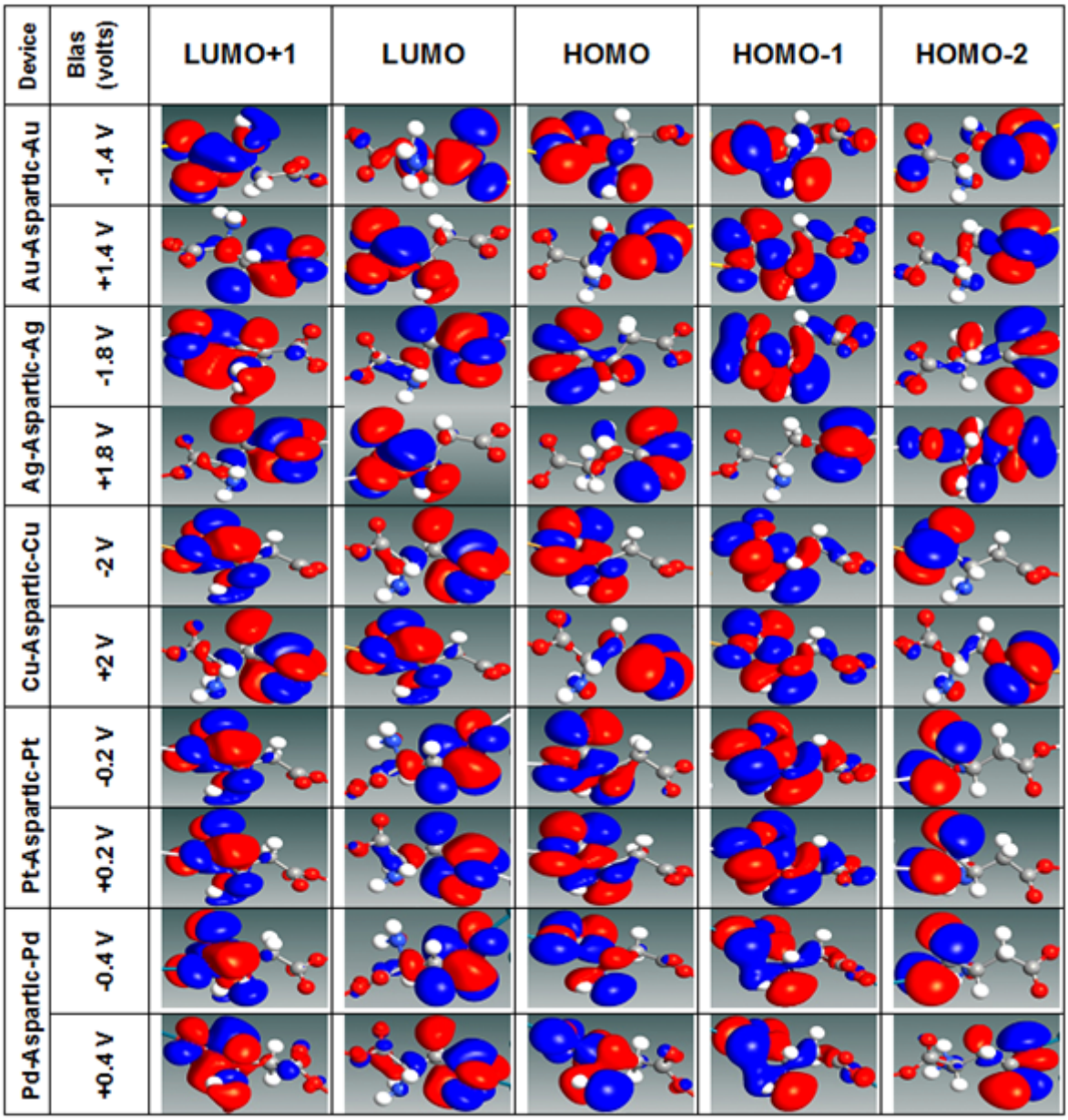

In case of Ag-Aspartic-Ag device, HOMO-1 of -1.8V shows the significant delocalization, due to presence of only bonding orbitals. Presence of only bonding or non-bonding molecular orbitals is more significant than combination of either with antibonding [87]. The HOMO-2 of +1.8 V in case of Ag-Aspartic-Ag device shows less favourable delocalization, due to the merging of bonding and antibonding orbitals. In case of Cu-Aspartic-Cu device, the HOMO and HOMO-1 at -2V shows more significant delocalization as compared to same combination (i.e. HOMO and HOMO-1) at +2V. In case of Pt-Aspartic-Pt device, the HOMO-1 at +0.2V depicts the more favourable delocalization as compared to HOMO-1 of -0.2V. In case of Pd-Aspartic-Pd device, the HOMO and HOMO-1 at +0.4V shows more delocalization as compared to the equivalent combination at -0.4V thus advocating the cause of rectification ratio. The enlarged view of delocalization in HOMO-1 of Pt-Aspartic-Pt at ±0.2V is shown in Fig. S1 to S2 in Supplementary files.

4. Conclusions

It is imperative to study various parameters of molecular junction in order to predict the application of bio-molecule in Nano electronic devices. To gain a deeper insight, it is necessary to discern the transport properties of bio-molecule in conjunction with different electrodes.

The transport behavior of L-aspartic acid (i.e., L-amino acid) bound to gold, silver, copper, platinum and palladium electrodes is observed by evaluating numerous factors including work function, tunnelling barrier, molecule-electrode coupling, conductance, I-V characteristics, NDR, rectification ratio, transmission spectra and MPSH. We perceive that the aspartic molecule offers the maximum coupling with platinum electrodes and minimum coupling with copper electrodes.

We observe the least conductance in Cu-Aspartic-Cu device at finite bias range of -2 to + 2V. This weak conductance confirms the weaker coupling of molecule with the electrode. Presences of conductance dip in Ag-Aspartic-Ag and Cu-Aspartic-Cu devices (shown in Fig. 2(b) and (c)) also confirm the weaker coupling of molecule with respective electrodes as compared to Pt-Aspartic-Pt devices. The conductance fluctuations in Pd-Aspartic-Pd is due to the transmission probability, in which fraction of the transmitted electrons are scattered back [88].

This molecule in all the molecular configurations exhibits remarkable NDR behaviour and reasonable rectification. Such behaviour is corroborated by studying transmission spectra and MPSH in details. L-aspartic molecule shows the highest rectification ratio of 3.20 (at ± 0.2 V) with platinum electrode. Single-molecule diode with rectification ratio less than 10, have also been reported by other researchers [89–92].

The molecule depicts the multiple NDR behaviour with all electrodes at different bias voltages. Although, glutamic acid is a similar negatively charged amino acid, yet it does not offer NDR using silver electrodes [26]. Ag-Aspartic-Ag molecular device offers two NDR regions in positive bias range. Highest peak to valley ratio (i.e. 1.38) is observed in case of Pt-Aspartic-Pt device. We also find the interesting behaviour of molecule that it offers equal number of NDR regions (i.e. 3 in each bias range) in Pd-Aspartic-Pd. Theoretically, NDR behaviour is also predicted in cysteine amino acid with Au (111), but detailed peak to valley ratio is not discussed [24]. Multiple NDR regions can also be observed in linear molecule by using nitro $(-\mathrm{NO}_2)$ end groups[93]. Theoretical prediction of NDR behavior in single molecule is experimentally validated by using scanning tunnelling microscopy[94].

These findings finally allow us to conclude the significance of molecule-electrode interface. Although the electrodes are symmetrical, yet there is visible NDR effects and significant rectification ratio. This asymmetrical behaviour can hence be explained in two ways. Firstly, the molecule contains the alkane (-CH2) side chain, which leads to the nonlinear effects in I-V characteristics [25, 26, 95]. Secondly, the molecule shows spatial asymmetric structure i.e., mirror symmetry is absent, which can also manifest nonlinear effects [23, 96].

The nonlinear effects can further be enhanced by asymmetrical molecule-electrode coupling which results into unequal shift of the Fermi levels of the electrodes [32, 97]. The detection of NDR effect in the molecule witnesses the potential applications of it in random access memory devices, oscillators, and

fast switching devices [98, 99]. Finite rectification ratio knocks the door to the future application in logic circuits and molecular memory[100]. We conclude from our theoretical findings that such biomolecule must need various experimental prospects with different electrodes. Different experimental approaches further gives the seal of approval to such biomolecule for future protein based electronics.

Declarations

Funding: The authors did not receive support from any organizations for the submitted work.

Conflicts of interests: The authors have no conflicts of interest to declare that are relevant to the content of this article.

Availability of data and material: Not Applicable

Code availability: Not Applicable

Conceptualization, Methodology, Writing-original draft preparation: Gaurav Sikri

Formal analysis and investigation, Writing-review and editing, Supervision: Ravinder Singh Sawhney

References

1. Amdursky N, Marchak D, Sepunaru L et al (2014) Electronic Transport via Proteins. Adv Mater. https://doi.org/10.1002/adma.201402304
2. Chi Q, Farver O, Ulstrup J (2005) Long-range protein electron transfer observed at the single-molecule level: In situ mapping of redox-gated tunneling resonance. Proc Natl Acad Sci U S A. https://doi.org/10.1073/pnas.0508257102
3. Alessandrini A, Facci P (2016) Electron transfer in nanobiodevices. Eur Polym J. https://doi.org/10.1016/j.eurpolymj.2016.03.028
4. Blumberger J (2015) Recent Advances in the Theory and Molecular Simulation of Biological Electron Transfer Reactions. Chem. Rev
5. Baldacchini C, Bizzarri AR, Cannistraro S (2016) Electron transfer, conduction and biorecognition properties of the redox metalloprotein Azurin assembled onto inorganic substrates. Eur. Polym. J
6. Livshits GI, Stern A, Rotem D et al (2014) Long-range charge transport in single G-quadruplex DNA molecules. Nat Nanotechnol. https://doi.org/10.1038/nnano.2014.246
7. Xiang L, Palma JL, Bruot C et al (2015) Intermediate tunnelling-hopping regime in DNA charge transport. Nat Chem. https://doi.org/10.1038/nchem.2183
8. Macchia E, Alberga D, Manoli K et al (2016) Organic bioelectronics probing conformational changes in surface confined proteins. Sci Rep. https://doi.org/10.1038/srep28085
9. Baîldea I (2013) Important insight into electron transfer in single-molecule junctions based on redox metalloproteins from transition voltage spectroscopy. J Phys Chem C.

https://doi.org/10.1021/jp408873c

10. Yamana K, Erbe A, Barton JK et al (2015) DNA Wires and Electron Transport Through DNA. In: DNA in Supramolecular Chemistry and Nanotechnology
11. Maruccio G (2012) Molecular electronics: Protein transistors strike gold. Nat. Nanotechnol
12. Rinaldi R, Biasco A, Maruccio G, et al (2002) Solid-state molecular rectifier based on self-organized metalloproteins. Adv Mater. https://doi.org/10.1002/1521-4095(20021016)14:20<1453::AID-ADMA1453>3.0.CO;2-C
13. Alfinito E, Reggiani L, Pousset J (2015) Proteotronics: Electronic devices based on proteins. In: Lecture Notes in Electrical Engineering
14. Wierzbinski E, Venkatramani R, Davis KL et al (2013) The single-molecule conductance and electrochemical electron-transfer rate are related by a power law. ACS Nano. https://doi.org/10.1021/nn401321k
15. Venkatramani R, Wierzbinski E, Waldeck DH, Beratan DN (2014) Breaking the simple proportionality between molecular conductances and charge transfer rates. Faraday Discuss. https://doi.org/10.1039/c4fd00106k
16. Ruiz MP, Aragonès AC, Camarero N et al (2017) Bioengineering a Single-Protein Junction. J. Am. Chem. Soc
17. Bostick CD, Mukhopadhyay S, Pecht I et al (2018) Protein bioelectronics: A review of what we do and do not know. Reports Prog. Phys
18. Wang H, Liu F, Dong T et al (2018) Charge-Transfer Knowledge Graph among Amino Acids Derived from High-Throughput Electronic Structure Calculations for Protein Database. ACS Omega. https://doi.org/10.1021/acsomega.8b00336
19. Oh S, Rubin JB, Bennett MVL et al (1999) Molecular determinants of electrical rectification of single channel conductance in gap junctions formed by connexins 26 and 32. J Gen Physiol. https://doi.org/10.1085/jgp.114.3.339
20. Ing NL, El-Naggar MY, Hochbaum AI (2018) Going the Distance: Long-Range Conductivity in Protein and Peptide Bioelectronic Materials. J. Phys. Chem. B
21. Metzger RM (2003) One-molecule-thick devices: Rectification of electrical current by three Langmuir-Blodgett monolayers. In: Synthetic Metals
22. Krzeminski C, Delerue C, Allan G et al (2001) Theory of electrical rectification in a molecular monolayer. Phys Rev B - Condens Matter Mater Phys. https://doi.org/10.1103/PhysRevB.64.085405
23. Reichert J, Ochs R, Beckmann D et al (2002) Driving Current through Single Organic Molecules. Phys Rev Lett. https://doi.org/10.1103/PhysRevLett.88.176804
24. Ganji MD, Aghaie H, Gholami MR (2008) Theoretical study of the electron transport through the cysteine amino acid nanomolecular wire. Int J Nanosci. https://doi.org/10.1142/s0219581x08005225

25. Zhou YH, Zheng XH, Xu Y, Zeng ZY (2006) Current rectification by asymmetric molecules: An ab initio study. J Chem Phys. https://doi.org/10.1063/1.2409689
26. Sikri G, Sawhney RS (2020) First principle approach to elucidate transport properties through l-glutamic acid-based molecular devices using symmetrical electrodes. J Mol Model. https://doi.org/10.1007/s00894-020-4323-x
27. Chothia C (1991) Asymmetry in protein structures. Ciba Found. Symp
28. Kojić-Prodić B, Štefanić Z (2010) Symmetry versus Asymmetry in the Molecules of Life: Homomeric protein assemblies. Symmetry (Basel). https://doi.org/10.3390/sym2020884
29. Honey CR, Miljkovic Z, Macdonald JF (1985) Ketamine and phencyclidine cause a voltage-dependent block of responses to l-aspartic acid. Neurosci Lett. https://doi.org/10.1016/0304-3940(85)90414-8
30. Teschke O, Soares DM (2016) Chiral Asymmetric Structures in Aspartic Acid and Valine Crystals Assessed by Atomic Force Microscopy. Langmuir. https://doi.org/10.1021/acs.langmuir.6b00092
31. Cordes M, Köttgen A, Jasper C et al (2008) Influence of amino acid side chains on long-distance electron transfer in peptides: Electron hopping via “stepping stones. Angew Chemie - Int Ed. https://doi.org/10.1002/anie.200705588
32. Zotti LA, Bednarz B, Hurtado-Gallego J et al (2019) Can one define the conductance of amino acids? Biomolecules. https://doi.org/10.3390/biom9100580
33. Ganji MD (2009) Density functional theory based treatment of amino acids adsorption on single-walled carbon nanotubes. Diam Relat Mater. https://doi.org/10.1016/j.diamond.2008.11.021
34. Li WQ, Huang B, Huang ML et al (2017) Detecting electron transport of amino acids by using conductance measurement. Sensors (Switzerland). https://doi.org/10.3390/s17040811
35. Zhao Y, Ashcroft B, Zhang P et al (2014) Single-molecule spectroscopy of amino acids and peptides by recognition tunnelling. Nat Nanotechnol. https://doi.org/10.1038/nnano.2014.54
36. Ohshiro T, Tsutsui M, Yokota K et al (2014) Detection of post-translational modifications in single peptides using electron tunnelling currents. Nat Nanotechnol. https://doi.org/10.1038/nnano.2014.193
37. An YP, Yang CL, Wang MS et al (2010) Ab initio investigations of the charge transport properties of endohedral M@C20 (M = Na and K) metallofullerenes. Chinese Phys B. https://doi.org/10.1088/1674-1056/19/11/113402
38. Shah A, Adhikari B, Martic S et al (2015) Electron transfer in peptides. Chem. Soc. Rev
39. Zotti LA, Cuevas JC (2018) Electron Transport Through Homopeptides: Are They Really Good Conductors? ACS Omega. https://doi.org/10.1021/acsomega.7b01917
40. Minoura N (1998) Nonlinear resistance behavior of current-voltage characteristics in polypeptide membranes with conformational transition. Langmuir. https://doi.org/10.1021/la970666f
41. Malaspina T, Fileti EE, Colherinhas G (2017) Elucidating the stability of bolaamphiphilic polypeptide nanosheets using atomistic molecular dynamics. Phys Chem Chem Phys. https://doi.org/10.1039/c7cp06284b

42. De Ferra F, Rodriguez F, Tortora O et al (1997) Engineering of peptide synthetases. Key role of the thioesterase-like domain for efficient production of recombinant peptides. J Biol Chem. https://doi.org/10.1074/jbc.272.40.25304
43. Deng XQ, Zhou JC, Zhang ZH et al (2009) Electrode metal dependence of the rectifying performance for molecular devices: A density functional study. Appl Phys Lett 95:103113. https://doi.org/10.1063/1.3205114
44. Cho Y, Kim WY, Kim KS (2009) Effect of electrodes on electronic transport of molecular electronic devices. J Phys Chem A 113:4100–4104. https://doi.org/10.1021/jp810467q
45. Parashar S, Srivastava P, Pattanaik M (2013) Electrode materials for biphenyl-based rectification devices. In: Journal of Molecular Modeling. Springer, pp 4467–4475
46. Natori K (2015) Nonideality of drain electrode and ballistic performance of MOSFET. Jpn J Appl Phys. https://doi.org/10.7567/JJAP.54.044102
47. Landauer R (2010) Spatial Variation of Currents and Fields Due to Localized Scatterers in Metallic Conduction. IBM J Res Dev. https://doi.org/10.1147/rd.13.0223
48. Xiang D, Jeong H, Lee T, Mayer D (2013) Mechanically controllable break junctions for molecular electronics. Adv. Mater
49. Mathew PT, Fang F (2018) Advances in Molecular Electronics: A Brief Review. Engineering
50. Böhler T, Grebing J, Mayer-Gindner A et al (2004) Mechanically controllable break-junctions for use as electrodes for molecular electronics. Nanotechnology. https://doi.org/10.1088/0957-4484/15/7/054
51. Burke K (2016) Improving Electronic Structure Calculations. Physics (College Park Md). https://doi.org/10.1103/physics.9.108
52. Van Mourik T, Bühl M, Gaigeot MP (2014) Density functional theory across chemistry, physics and biology. Philos Trans R Soc A Math Phys Eng Sci. https://doi.org/10.1098/rsta.2012.0488
53. Smidstrup S, Markussen T, Vancraeyveld P et al (2020) QuantumATK: An integrated platform of electronic and atomic-scale modelling tools. J Phys Condens Matter 32:15901
54. Perdew JP, Burke K, Ernzerhof M (1996) Generalized gradient approximation made simple. Phys Rev Lett 77:3865–3868. https://doi.org/10.1103/PhysRevLett.77.3865
55. Xu X, Goddard WA (2004) The extended Perdew-Burke-Ernzerhof functional with improved accuracy for thermodynamic and electronic properties of molecular systems. J Chem Phys. https://doi.org/10.1063/1.1771632
56. Kaschner R, Hohl D (1998) Density functional theory and biomolecules: A study of glycine, alanine, and their oligopeptides. J Phys Chem A. https://doi.org/10.1021/jp980975u
57. Zhang Z, Xu Z, Yang Z et al (2013) The stabilization effect of dielectric constant and acidic amino acids on arginine-arginine (Arg-Arg) pairings: Database survey and computational studies. J Phys Chem B. https://doi.org/10.1021/jp4001658

58. Chen X, Gao P, Guo L, Zhang S (2015) Graphdiyne as a promising material for detecting amino acids. Sci Rep. https://doi.org/10.1038/srep16720
59. Saffari M, Mohebpour MA, Rahimpour Soleimani H, Bagheri Tagani M (2017) DFT analysis and FDTD simulation of CH3NH3PbI3-xClx mixed halide perovskite solar cells: Role of halide mixing and light trapping technique. J Phys D Appl Phys. https://doi.org/10.1088/1361-6463/aa83c8
60. Troullier N, Martins JL (1991) Efficient pseudopotentials for plane-wave calculations. Phys Rev B. https://doi.org/10.1103/PhysRevB.43.1993
61. De Waele S, Lejaeghere K, Sluydts M, Cottenier S (2016) Error estimates for density-functional theory predictions of surface energy and work function. Phys Rev B. https://doi.org/10.1103/PhysRevB.94.235418
62. Niemantsverdriet JW (2007) Appendix: Metal Surfaces and Chemisorption. Spectrosc Catal 297–320. https://doi.org/10.1002/9783527611348.app1
63. Derry GN, Kern ME, Worth EH (2015) Recommended values of clean metal surface work functions. J Vac Sci Technol A Vacuum Surfaces Film. https://doi.org/10.1116/1.4934685
64. Chelvayohan M, Mee CHB (1982) Work function measurements on (110), (100) and (111) surfaces of silver. J Phys C Solid State Phys. https://doi.org/10.1088/0022-3719/15/10/029
65. Patra A, Bates JE, Sun J, Perdew JP (2017) Properties of real metallic surfaces: Effects of density functional semilocality and van der Waals nonlocality. Proc Natl Acad Sci U S A. https://doi.org/10.1073/pnas.1713320114
66. Bocquet ML, Rappe AM, Dai HL (2005) A density functional theory study of adsorbate-induced work function change and binding energy: Olefins on Ag(111). Mol Phys 103:883–890. https://doi.org/10.1080/00268970412331333609
67. Sun J, Remsing RC, Zhang Y et al (2016) Accurate first-principles structures and energies of diversely bonded systems from an efficient density functional. Nat Chem. https://doi.org/10.1038/nchem.2535
68. Farnsworth HE, Winch RP (1940) Photoelectric work functions of (100) and (111) faces of silver single crystals and their contact potential difference. Phys Rev 58:812–819. https://doi.org/10.1103/PhysRev.58.812
69. Tran R, Li XG, Montoya JH et al (2019) Anisotropic work function of elemental crystals. Surf Sci 687:48–55. https://doi.org/10.1016/j.susc.2019.05.002
70. Haas GA, Thomas RE (1977) Work function and secondary emission studies of various Cu crystal faces. J Appl Phys 48:86–93. https://doi.org/10.1063/1.323329
71. Salmern M, Ferrer S, Jazzar M, Somorjai GA (1983) Photoelectron-spectroscopy study of the electronic structure of Au and Ag overlayers on Pt(100), Pt(111), and Pt(997) surfaces. Phys Rev B 28:6758–6765. https://doi.org/10.1103/PhysRevB.28.6758
72. Da Silva JLF, Stampfl C, Scheffler M (2006) Converged properties of clean metal surfaces by all-electron first-principles calculations. Surf Sci 600:703–715. https://doi.org/10.1016/j.susc.2005.12.008

73. Fischer R, Schuppler S, Fischer N et al (1993) Image states and local work function for Ag/Pd(111). Phys Rev Lett 70:654–657. https://doi.org/10.1103/PhysRevLett.70.654
74. Giese TJ, York DM (2010) Density-functional expansion methods: Evaluation of LDA, GGA, and meta-GGA functionals and different integral approximations. J Chem Phys. https://doi.org/10.1063/1.3515479
75. Jakobi K (2005) 3.1.2.4 Work function data. In: Electronic and Vibrational Properties. Springer-Verlag, pp 56–68
76. Pescia D, Meier F (1982) Spin polarized photoemission from gold using circularly polarized light. Surf Sci 117:302–309. https://doi.org/10.1016/0039-6028(82)90512-X
77. Fall C, Binggeli N, Baldereschi A (2000) Work-function anisotropy in noble metals: Contributions from d states and effects of the surface atomic structure. Phys Rev B - Condens Matter Mater Phys 61:8489–8495. https://doi.org/10.1103/PhysRevB.61.8489
78. Singh-Miller NE, Marzari N (2009) Surface energies, work functions, and surface relaxations of low-index metallic surfaces from first principles. Phys Rev B - Condens Matter Mater Phys 80:235407. https://doi.org/10.1103/PhysRevB.80.235407
79. Engelkes VB, Beebe JM, Frisbie CD (2004) Length-dependent transport in molecular junctions based on SAMs of alkanethiols and alkanedithiols: Effect of metal work function and applied bias on tunneling efficiency and contact resistance. J Am Chem Soc 126:14287–14296. https://doi.org/10.1021/ja046274u
80. Xie Z, Bâldea I, Smith CE et al (2015) Experimental and Theoretical Analysis of Nanotransport in Oligophenylene Dithiol Junctions as a Function of Molecular Length and Contact Work Function. ACS Nano 9:8022–8036. https://doi.org/10.1021/acsnano.5b01629
81. Van Wees BJ, Van Houten H, Beenakker CWJ et al (1988) Quantized conductance of point contacts in a two-dimensional electron gas. Phys Rev Lett. https://doi.org/10.1103/PhysRevLett.60.848
82. van Houten H, Beenakker CWJ, Staring AAM (1992) Coulomb-Blockade Oscillations in Quantum Wires and Dots
83. Yacoby A, Stormer HL, Wingreen NS et al (1996) Nonuniversal conductance quantization in quantum wires. Phys Rev Lett. https://doi.org/10.1103/PhysRevLett.77.4612
84. Apel W, Rice TM (1982) Combined effect of disorder and interaction on the conductance of a one-dimensional fermion system. Phys Rev B. https://doi.org/10.1103/PhysRevB.26.7063
85. Wang K, Xu B (2017) Modulation and Control of Charge Transport Through Single-Molecule Junctions. Top Curr Chem 375:. https://doi.org/10.1007/s41061-017-0105-z
86. Beebe JM, Engelkes VB, Miller LL, Frisbie CD (2002) Contact resistance in metal-molecule-metal junctions based on aliphatic SAMs: Effects of surface linker and metal work function. J Am Chem Soc 124:11268–11269. https://doi.org/10.1021/ja0268332
87. Bingham RC (1976) The Stereochemical Consequences of Electron Delocalization in Extended π Systems. An Interpretation of the Cis Effect Exhibited by 1,2-Disubstituted Ethylenes and Related Phenomena. J Am Chem Soc. https://doi.org/10.1021/ja00418a036

88. Ludoph B, van Ruitenbeek JM (2000) Conductance fluctuations as a tool for investigating the quantum modes in atomic-size metallic contacts. Phys Rev B - Condens Matter Mater Phys. https://doi.org/10.1103/PhysRevB.61.2273
89. Elbing M, Ochs R, Koentopp M et al (2005) A single-molecule diode. Proc Natl Acad Sci U S A 102:8815–8820. https://doi.org/10.1073/pnas.0408888102
90. Díez-Pérez I, Hihath J, Lee Y et al (2009) Rectification and stability of a single molecular diode with controlled orientation. Nat Chem 1:635–641. https://doi.org/10.1038/nchem.392
91. Lörtscher E, Gotsmann B, Lee Y et al (2012) Transport properties of a single-molecule diode. ACS Nano 6:4931–4939. https://doi.org/10.1021/nn300438h
92. Batra A, Darancet P, Chen Q et al (2013) Tuning rectification in single-molecular diodes. Nano Lett 13:6233–6237. https://doi.org/10.1021/nl403698m
93. Min Y, Zhuang GC, Yao KL (2020) Multiple negative differential resistance in nitro-based two-probe molecular junction. Phys Lett Sect A Gen At Solid State Phys. https://doi.org/10.1016/j.physleta.2020.126720
94. Dagar P, Bera J, Vyas G, Sahu S (2019) Bidirectional multiple negative differential resistance (BM-NDR): An interplay between interface resistance and redox reaction. Org Electron. https://doi.org/10.1016/j.orgel.2019.05.031
95. Larade B, Bratkovsky AM (2003) Current rectification by simple molecular quantum dots: An ab initio study. Phys Rev B - Condens Matter Mater Phys. https://doi.org/10.1103/PhysRevB.68.235305
96. Cahn RS, Ingold CK, Prelog V (1956) The specification of asymmetric configuration in organic chemistry. Experientia. https://doi.org/10.1007/BF02157171
97. Zhao J, Yu C, Wang N, Liu H (2010) Molecular rectification based on asymmetrical molecule-electrode contact. J Phys Chem C. https://doi.org/10.1021/jp905713a
98. Nam Do V, Dollfus P (2010) Negative differential resistance in zigzag-edge graphene nanoribbon junctions. In: Journal of Applied Physics
99. Kim KH, Park HY, Shim J et al (2020) A multiple negative differential resistance heterojunction device and its circuit application to ternary static random access memory. Nanoscale Horizons. https://doi.org/10.1039/c9nh00631a
100. Zhou Y, Qiu N, Li R et al (2016) Negative differential resistance and rectifying performance induced by doped graphene nanoribbons p-n device. Phys Lett Sect A Gen At Solid State Phys. https://doi.org/10.1016/j.physleta.2016.01.010

Figures

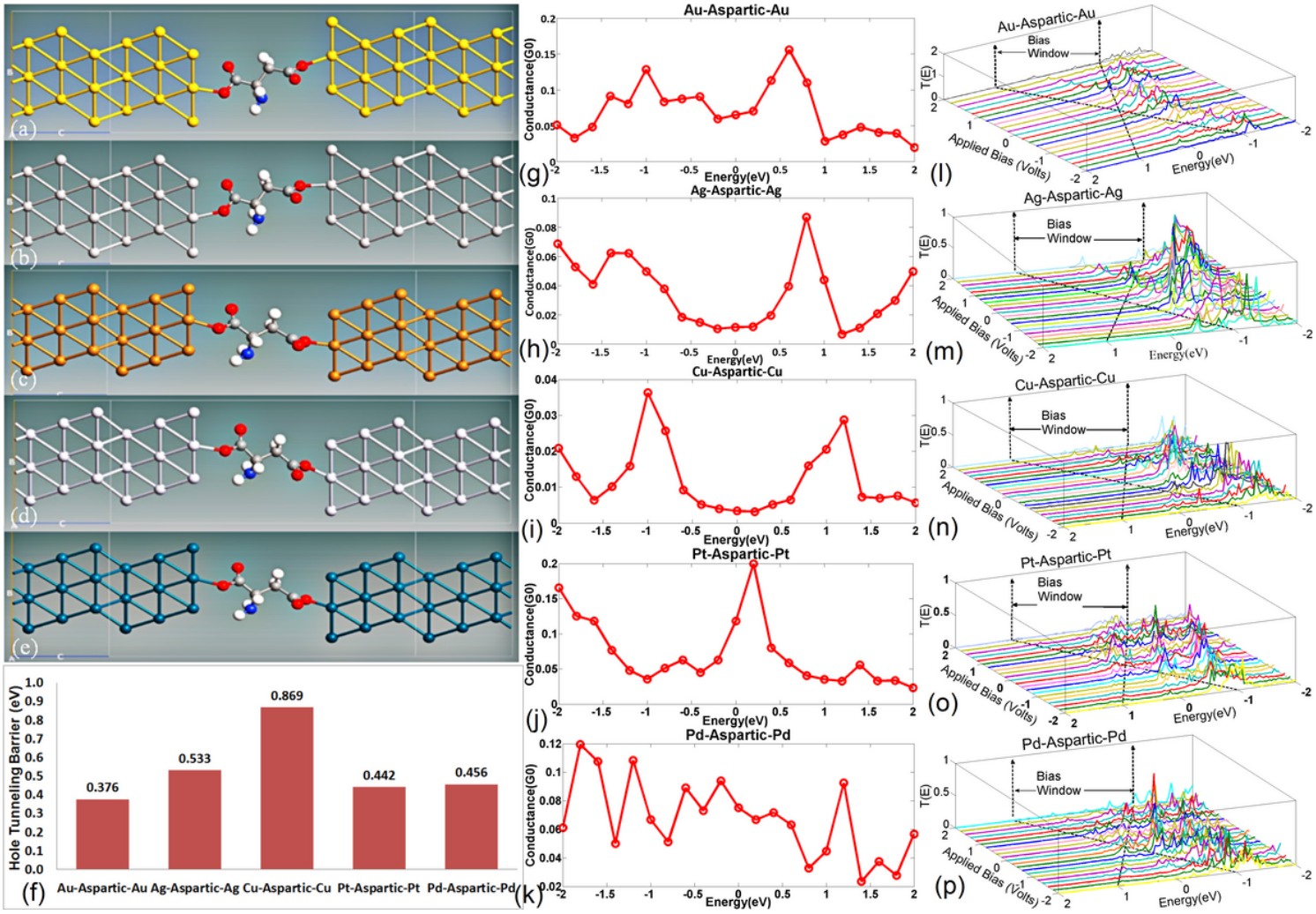

Figure 1

(Color Online): L-Aspartic acid stringed to (a) Gold, (b) Silver, (c) Copper, (d) Platinum and (e) Palladium electrodes with central scattering region consisting of 3 layers of electrodes on each side. (f) Hole tunnelling barrier of different molecular devices. Conductance expressed in units of Quantum of conductance (G0) changes with change in bias voltage from -2V to + 2V in (g) Au-Aspartic-Au, (h) Ag-Aspartic-Ag, (i) Cu-Aspartic-Cu, (j) Pt-Aspartic-Pt and (k) Pd-Aspartic-Pd. Three-dimensional transmission spectra of (l) Au-Aspartic-Au device, (m) Ag-Aspartic-Ag device, (n) Cu-Aspartic-Cu device, (o) Pt-Aspartic-Pt device and (p) Pd-Aspartic-Pd device at bias range of -2 to +2V

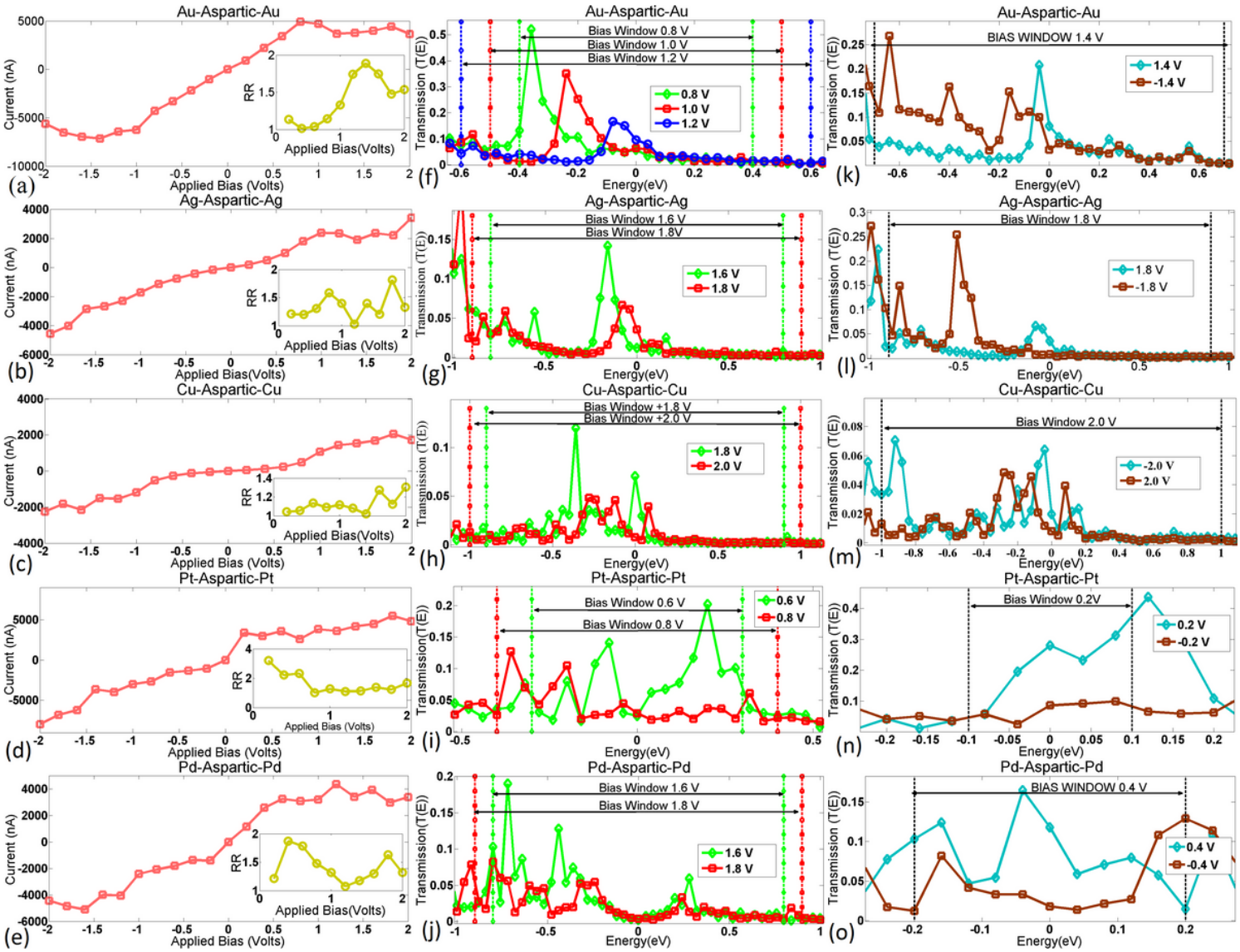

Figure 2

(Color online) I-V characteristics of (a) Au-Aspartic-Au, (b) Ag-Aspartic-Ag, (c) Cu-Aspartic-Cu, (d) Pt-Aspartic-Pt and (e) Pd-Aspartic-Pd devices. The inset shows the rectification ratio of respective devices. Inspection of Negative differential resistance of (f) Au-Aspartic-Au, (g) Ag-Aspartic-Ag, (h) Cu-Aspartic-Cu, (i) Pt-Aspartic-Pt and (j) Pd-Aspartic-Pd using Transmission Spectra. Elucidation of Rectification ratio of (k) Au-Aspartic-Au, (l) Ag-Aspartic-Ag, (m) Cu-Aspartic-Cu, (n) Pt-Aspartic-Pt and (o) Pd-Aspartic-Pd using Transmission Spectra

Supplementary Files

This is a list of supplementary files associated with this preprint. Click to download.

- GraphicalAbstract.png
- SupplementaryFileNDRRRAsparticacid.docx